Extended Abstracts of the 2019 International Conference on Solid State Devices and Materials, Nagoya, 2019, pp935-936

Low-temperature Ge/Si interstitials-mediated local densification and nanocrystallization of CVD Si_3N_4 for advanced Si photonics and electronics

K. P. Peng, T. L. Huang, T. George, H. C. Lin, and Pei-Wen Li

Institute of Electronics Engineering, National Chiao Tung University
1001 University Road, Hsinchu, Taiwan
E-mail: pwli@nctu.edu.tw

Abstract

We reported a unique, local densification and even nanocrystallization of low-pressure chemical vapor deposited (LPCVD) amorphous Si_3N_4 layers, that is catalytically-mediated by Ge quantum dots (QDs) and Si interstitials in close proximity to the Si_3N_4 layers during thermal oxidation in an H_2O ambient at 900ºC. The densification of Si_3N_4 layers appears to be achieved by a phase transition from the amorphous to the nanocrystalline state and are influenced by the oxidation time and Ge QD size. Implications of the highly localized, nanoscale densification and crystallization of silicon-nitride (Si_3N_4) layers for photonic and electronic device applications are discussed.

1. Introduction

Silicon nitride (Si_3N_4) films deposited by CVD techniques have been recognized as a fully-CMOS compatible platform for electronics and photonics integrated circuits for their wide-ranging applications such as insulating spacers, tensile stressors, and charge trapping centers for MOSFETs/memory as well as hybrid photonic devices of waveguides, wavelength filters, optical frequency combs and antireflection coatings. However, in practice, long-duration, high temperature (~1200 °C for at least 3 h) densification of Si_3N_4 is generally required in order to improve the high density of crystalline imperfections in the CVD Si_3N_4 films so as to reduce leakage current and optical absorption loss. The key problem with such an extremely high-temperature, long-duration densification process is that the Si_3N_4 film is prone to crack formation due to the large thermal stresses that are generated within the film, which is detrimental to achieving high-performance Si electronics-photonics co-integration

In this paper, we report our experimental observation of a unique, local densification and nanocrystallization of LPCVD amorphous Si_3N_4 films. The local densification and nanocrystallization is catalytically-mediated by Ge quantum dots (QDs) in close proximity to the Si_3N_4 film during thermal oxidation in an H_2O ambient at 900ºC. The densification of Si_3N_4 appears to be achieved by a phase transition from the amorphous to the nanocrystalline state as evidenced by energy dispersive *x*-ray spectroscopy (EDX), electron energy loss spectroscopy (EELS), nanobeam diffraction (NBD) and high-angle annular dark-field imaging (HAADF) scanning transmission electron microscopy (STEM) observations.

2. Experimental

A serendipitous discovery occurred when we attempted to produce Ge quantum dots (QDs) embedded within a **Si_3N_4/Si** ridge. The fabrication started with the growth of 10nm-thick SiO_2 in an H_2O ambient at 900ºC followed by the deposition of a 40nm-thick poly-Si layer using LPCVD at 620ºC over Si substrates. Nano-patterned poly-Si ridges were subsequently produced using a combination of electron-beam lithography and SF_6/C_4F_8 plasma etching (Fig. 1(a)). Next, a bi-layer of 25nm-thick Si_3N_4 and 30nm-thick poly-$Si_{0.85}Ge_{0.15}$ was sequentially deposited using LPCVD (Fig. 1(b)) in order to have conformal coverage over the previously nano-patterned, poly-Si ridges. Subsequently, a direct etch-back process produced symmetrical spacers of poly-$Si_{0.85}Ge_{0.15}$ at each ridge sidewall (Fig. 1(c)). Then, a second lithography patterning step was used to define the poly-$Si_{0.85}Ge_{0.15}$ islands (Fig. 1(d)). Finally, thermal oxidation at 900ºC in an H_2O ambient was performed to form two spherical Ge QDs (Fig. 1(e)) at each sidewall corner of the ridges.

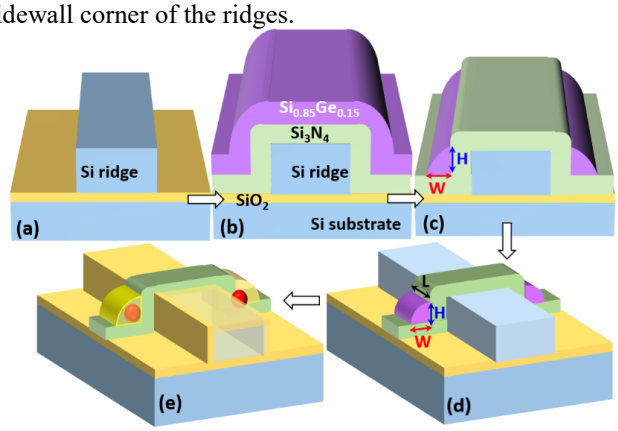

Fig. 1Process flow for the fabrication of double QDs embedded within SiO_2/Si_3N_4 matrices via the thermal oxidation of SiGe spacer islands nano-patterned over a bilayer of Si_3N_4/poly-Si. (a) Poly-Si ridges were lithographically-patterned over buffer layers of SiO_2 on top of Si substrate. (b) Sequential deposition of Si_3N_4 and poly-$Si_{0.85}Ge_{0.15}$ layers conformally encapsulating over the poly-Si ridges. (c) Symmetrical spacer stripes of poly-$Si_{0.85}Ge_{0.15}$ were formed at each sidewall of the Si_3N_4/poly-Si ridges by a direct SF_6/C_4F_8 plasma etch back process. (d) Symmetrical poly-$Si_{0.85}Ge_{0.15}$ spacer islands were produced by lithographically-patterning processes across the spacer stripes of poly-$Si_{0.85}Ge_{0.15}$. (e) A pair of spherical Ge QDs were formed at each sidewall corner of nano-patterned Si_3N_4/poly-Si ridge by thermal oxidation at 900ºC for 10–27min.

3. Results and Discussion

We observed from extensive STEM examinations (Figure 2(a)) that following 900ºC, 10min thermal oxidation of poly-

$Si_{0.85}Ge_{0.15}$ islands at the sidewalls of Si_3N_4/poly-Si nano-ridges, not only spherical Ge QDs were formed at each sidewall corner of the Si_3N_4/Si nano-ridges, but also high-contrast regions appear in the STEM micrographs within the Si_3N_4 layers at the concave corners of the ridge where the Ge QDs penetrate. An important finding of note from the EDX maps shown in Figure 2(a) is a remarkable correlation in the shapes of the high-contrast STEM regions and the intensification of the Nitrogen, Si and decrease of Oxygen x-ray fluorescence (XRF) intensities within the EDX elemental maps. The significant enhancements in XRF intensity for both N and Si is a clear indication of the densification of Si_3N_4 within the observed STEM high-contrast regions, whereas a corresponding decrease in the O XRF intensity indicates an expulsion of O from the densified regions. Also, notably, the Ge signal is undetectable within these high-contrast STEM regions, which is consistent with the low solubility of Ge within Si_3N_4. Another important observation made from the combined STEM micrographs and EDX maps shown in the Figure 2(b) series is that the high contrast is further intensified for the regions associated with enhanced incorporation of N and Si for longer duration thermal oxidation (27min).

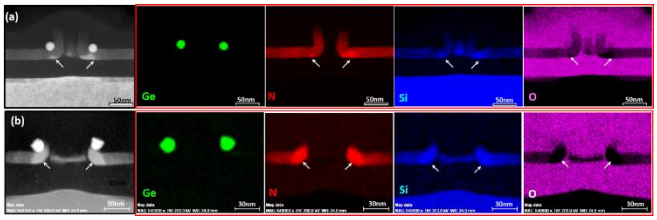

Fig. 2 Series of images containing STEM micrographs (far left) and EDX maps of Ge, N, Si and O elemental distributions for a pair of Ge QDs with diameter of 20nm formed at each sidewall of the ridges after thermal oxidation of poly-SiGe spacer islands near the corners of Si_3N_4/Si nano-ridges at 900 ºC for (a) 10min and (b) 27min. Arrows in the STEM and EDX maps highlight the densification of Si_3N_4 within the STEM high-contrast regions corresponding to significant enhancements in XRF intensity for both N and Si accompanied by a corresponding decrease in O XRF intensity. Also, (b) the Si_3N_4 densification is enhanced by increasing the thermal oxidation time.

All STEM and EDX map observations point to the highly-localized densification of the high-contrast Si_3N_4 regions. Figure 3 contains the EELS maps (Fig. 3(a)), spectra, and linescans along the Si_3N_4 layer for conditions with or without the Ge QD in close proximity. No chemical shift was observed in the K-edge signal of Nitrogen for the entire Si_3N_4 layer (Fig. 3(b)), suggesting no changes in the binding energy and the chemical composition of the Si_3N_4 layer. It is clearly seen in Figure 3(c) that compared to the case of the Si_3N_4 layer away from the Ge QDs, a significant enhancement in density by a factor of 2.2 and 1.3 for N and Si, respectively, occurs for the high-contrast Si_3N_4 regions.

Notably, the local densification of Si_3N_4 in close proximity of the Ge QD (Fig. 4(a)) is associated with the nanocrystallization of Si_3N_4 as evidenced by the appearance of spotty diffraction rings (Fig. 4(b)) in contrast to the blurred and diffuse diffraction rings for the amorphous Si_3N_4 (Fig. 4(c)) away from the Ge QDs.

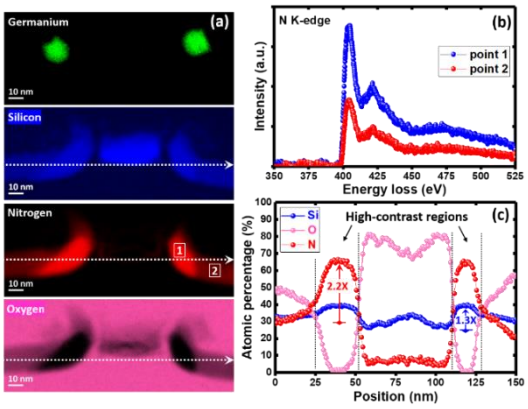

Fig. 3 EELS (a) maps, (b) spectra, and (c) linescans along the Si_3N_4 layer in close proximity of the Ge QDs. (c) The chemical composition of the Si_3N_4 layer remains unchanged for the entire Si_3N_4 layer since no chemical shift was observed in the K-edge of Nitrogen for EELS spectra taken at point 1 in the high-contrast Si_3N_4 region in close proximity of the penetrating Ge QDs as well as at point 2 for the lower density Si_3N_4 layer away from the Ge QD. The EELS linescans along the Si_3N_4 layer (as denoted by the white arrow) shows a large enhancement in the density for both N and Si accompanied by a corresponding decrease in the O intensity for the high-contrast Si_3N_4 regions in comparison to the Si_3N_4 layer regions away from the Ge QD.

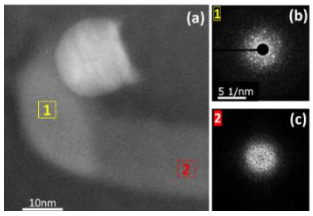

Fig. 4 (a) HAADF STEM of the Ge QDs penetrating Si_3N_4 encapsulation layers showing clear lattice fringes for the Ge QD. Nanobeam Diffraction patterns taken for (b) the densified Si_3N_4 layer in close proximity of the Ge QD (point 1) and (c) for the amorphous Si_3N_4 layer away from the Ge QD (point 2). The appearance of spotty diffraction rings is a testament to the phase transition of the high-contrast Si_3N_4 regions from the amorphous to polycrystalline state.

3. Conclusions

We have observed a unique local densification of Si_3N_4 layers mediated by the presence of Ge and Si interstitials at significantly lower temperatures than was previously possible. The densification of LPCVD-Si_3N_4 is achieved by an increase in Si and N concentrations and reduction in O concentration accompanying the phase transition from the amorphous to nanocrystalline state. The local densification of Si_3N_4 is enhanced by the presence of larger Ge QDs and by longer oxidation times. The local densification of Si_3N_4 enabled by "burrowing" Ge QDs and proximal Si layers has been demonstrated to improve gate leakage and to reduce interface-state density for the resulting Ge-QD/SiO_2/SiGe MOSFETs. We envisage further scientific exploration of this unique densifications of Si_3N_4 for boosting the performance of advanced CMOS electronics-photonics co-integration.

Acknowledgements

This work was supported by MOST 105-2221- E-009-134-MY3 and 108-2633-E-009-001, Taiwan, R. O. C.